

# Does the Amati Correlation Exhibit Redshift-Driven Heterogeneity in Long GRBs?

Darshan Singh<sup>a,b</sup> Meghendra Singh<sup>c</sup> Dinkar Verma<sup>a</sup> Kanhaiya Lal Pandey<sup>d</sup> Shashikant Gupta<sup>a</sup>

<sup>a</sup>Department of Basic and Applied Sciences, GD Goenka University, Gurugram, 122103, India.

<sup>b</sup>Department of Physics, Mata Raj Kaur Institute of Engineering and Technology, Rewari, 123401, India.

<sup>c</sup>Delhi Metro Rail Corporation Limited, New Delhi, 110001, India.

<sup>d</sup>Department of Physics, School of Advanced Sciences, Vellore Institute of Technology, Vellore, 632014, India.

E-mail: [shashikantgupta.astro@gmail.com](mailto:shashikantgupta.astro@gmail.com)

**Abstract.** Long gamma-ray bursts (GRBs) offer significant insights into cosmology due to their high energy emissions and the potential to probe the early universe. The Amati relation, which links the intrinsic peak energy to the isotropic energy, is crucial for understanding their cosmological applications. This study investigates the redshift-driven heterogeneity of the Amati correlation in long GRBs. Analyzing 221 long GRBs with redshifts from 0.034 to 8.2 we divided the dataset based on redshift thresholds of 1.5 and 2. Using Bayesian marginalization and Reichart's likelihood approach, we found significant differences in the Amati parameters between low and high redshift subgroups. These variations, differing by approximately  $2\sigma$  at  $z = 1.5$  and more than  $1\sigma$  at  $z = 2$ , suggest an evolution in the GRB population with redshift, possibly reflecting changes in host galaxy properties. However, selection effects and instrumental biases may also contribute. Our results challenge the assumption of the Amati relation's universality and underscore the need for larger datasets and more precise measurements from upcoming missions like THESEUS and eXTP to refine our understanding of GRB physics.

**Keywords:** Cosmology, Gamma Ray Burst, Large-scale structure of the universe, galaxies, high redshift

---

## Contents

<b>1</b>	<b>Introduction</b>	<b>1</b>
<b>2</b>	<b>Data and Methodology</b>	<b>2</b>
2.1	GRB Data Sample	2
2.2	Methodology	3
2.3	Distribution of Low and High- $z$ GRBs Across the Sky	4
2.4	Intrinsic Scatter	5
<b>3</b>	<b>Results and Discussion</b>	<b>6</b>
3.1	Main Results	9
3.2	Probable Instrumental Biases and Selection Effects	10
3.3	Low- $z$ vs High- $z$ GRB Hosts	10
<b>4</b>	<b>Conclusions</b>	<b>11</b>

---

## 1 Introduction

Gamma-ray bursts (GRBs), observed as intense flashes of gamma rays in distant galaxies, represent some of the most energetic explosions in the universe [1, 2]. A key characteristic of GRBs is their pulse duration, commonly quantified by the parameter  $T_{90}$  [3], defined as the time interval during which 90% of the total background-subtracted gamma-ray photons are detected. Based on  $T_{90}$ , GRBs are classified into two main types: short GRBs, lasting less than 2 seconds and typically resulting from the merger of compact objects like neutron stars or black holes; and long GRBs, lasting more than 2 seconds and believed to be associated with the collapse of massive stars into black holes [2, 4]. Long GRBs are particularly valuable for cosmological studies due to their longer pulse duration, facilitating localization within their host galaxies and redshift measurement. They can measure cosmological distances, probe the early universe, and provide constraints on cosmic reionization and star formation rates. Correlations among various GRB observables are important to calibrate the observational data for distance measurement. Among the various correlations observed, the Amati relation [5–8], which links the intrinsic peak energy ( $E_{peak}$ ) in the  $\nu F_\nu$  spectrum of a burst to its equivalent isotropic energy ( $E_{iso}$ ), has been a subject of particular interest. Originally expressed in exponential form, the relation is now commonly presented in linear form for its elegance:

$$\log E_{iso} = a + b \log E_{p,i}, \quad (1.1)$$

where the intercept,  $a$  and the slope,  $b$  are known as Amati parameters. The parameter  $b$  is usually positive indicating a positive correlation between  $E_{iso}$  and  $E_{p,i}$  while  $a$  is negative. Alongside the Yonetoku relation between  $E_{peak}$  and the isotropic peak luminosity,  $L_{iso}$  [9]; Ghirlanda relation between  $E_{peak}$  and collimation-corrected energy,  $E_\gamma$  [10, 11]; and Dianotti relation [12]; Amati relation serves as a cornerstone for probing the physics of GRBs and their use as cosmological tools [13–16].

Several studies have attempted to constrain cosmological parameters using GRB data [17–20]. However, a critical question arises regarding whether the relations used for cosmological applications remain constant throughout the history of the universe or evolve with

redshift, a measure of the cosmic scale and the age of the universe at the time of the burst [21]. GRBs are calibrated using type Ia supernovae for cosmological applications, which can be observed only up to  $z = 1.75$ . If high-redshift GRBs differ from their low-redshift counterparts, their calibration may be questionable. Recent studies have presented conflicting views on the evolution of the Amati parameters with redshift. Some research suggests that the Amati parameters,  $a$  and  $b$ , may systematically vary with the mean redshift of GRBs. By dividing a sample of long-duration GRBs into redshift-based groups and fitting the Amati relation separately to each group, significant and systematic changes in the parameters with redshift have been observed [13, 14, 17, 22–25]. Monte Carlo simulations further support that this variation is unlikely due to selection effects from the fluence limit, indicating a strong evolution of GRBs with cosmological redshift [23]. Conversely, other studies [26, 27] challenge this view by using different samples of GRBs and investigating the redshift independence of the Amati and Yonetoku relations. By binning the data by redshift and fitting both relations, these studies found that the normalization and slope do not exhibit systematic evolution with redshift, implying that the Amati and Yonetoku relations are redshift-independent. The discrepancy between these findings raises important questions about the intrinsic properties of GRBs and their use as standard candles in cosmology.

Differences in the properties of GRBs at different redshifts may reflect signatures of galaxy evolution. Substantial evidence indicates evolutionary shifts in the demographics of various galaxy morphologies with increasing redshift. Notably, there is a significant decline in the proportion of disk galaxies around  $z = 2$ , accompanied by a corresponding increase in peculiar types. However, for massive galaxies, the fractions of disks, spheroids, and peculiar types appear to remain relatively constant within the redshift range of  $1.5 < z < 6.5$ . Furthermore, galaxy morphologies exhibit limited correlation with other key physical properties such as star formation rate, colour, mass, or size [28–30]. [31] investigated the mass distribution of host galaxies of long GRBs and the redshift distribution of long GRBs, indicating that GRB host galaxies are metallicity-biased tracers of star formation. At high redshift, the early-type galaxies can be observed in the active star formation period, during which massive star explosions and galactic winds occur. This situation is not found at lower redshift, where star formation is already quenched for this morphological type [32] which might be linked to a low GRB rate.

To address this knowledge gap, i.e., whether there are two different populations of long GRBs at low and high redshifts, this study investigates the differences in Amati parameters in the low and high- $z$  regimes. In Section 2, we will describe our methodology, including the data and the analysis techniques employed. Section 3 presents the key findings of our research and discusses the implications of these findings. Finally, Section 4 will conclude the paper by summarizing the main points and suggesting avenues for future research.

## 2 Data and Methodology

### 2.1 GRB Data Sample

Investigating the evolution of GRBs with redshift requires large datasets of long GRBs covering a wide range of redshifts. In a previous study, [22] used 162 long GRBs compiled by [19] to explore differences between low and high-redshift GRB populations. In the current study, we utilize a larger and more recent dataset with precise photometric and spectroscopic information. This dataset, containing 221 long GRBs and covering the redshift range

**Table 1:** Description of GRB data and its subgroups. Groups  $G_1$  and  $G_2$  belong to the division at  $z = 1.5$ , while  $G'_1$  and  $G'_2$  belong to the division at  $z = 2$ .

Group(s)	Number of GRBs	$z_{min}$	$z_{max}$	Median $z$
G	221	0.034	8.20	1.62
$G_1$	100	0.034	1.19	0.89
$G_2$	121	1.517	8.20	2.45
$G'_1$	132	0.034	1.98	1.10
$G'_2$	89	2.006	8.20	2.77

$0.034 \leq z \leq 8.2$ , is readily available [17]. This dataset primarily derives from the joint observations conducted by Swift and Fermi. In some cases,  $E_{p,i}$  is provided directly by Swift/BAT. The Swift satellite has significantly contributed to detecting several GRBs with their redshifts. Swift is equipped with three instruments: the Burst Alert Telescope (BAT) for GRB detection, the X-ray Telescope (XRT), and the Ultra-Violet and Optical Telescope (UVOT). BAT, with its large field of view, detects GRBs in the energy range of 15 keV to 150 keV. Upon detection, the satellite slews to the burst direction for XRT and UVOT observations. The energy range of XRT is 0.2-10 keV, while the UVOT is capable of observations in the 170 – 600 nm wavelength range [33].

The Fermi Gamma-Ray Space Telescope (FGST), launched by NASA in 2008, has become a cornerstone in the study of high-energy gamma rays [34]. The primary instrument onboard FGST is the Large Area Telescope (LAT), a high-energy gamma-ray imaging telescope with a wide field of view, operating in the energy range from below 20 MeV to more than 300 GeV. Additionally, Fermi is equipped with the Gamma-ray Burst Monitor (GBM) and the Anticoincidence Detector (ACD), which complement the observations made by the LAT. The LAT provides unprecedented sensitivity across a broad energy range, spanning approximately 20 MeV to 300 GeV, making Fermi an invaluable tool in high-energy astrophysics.

## 2.2 Methodology

As discussed in Section 1, galaxy populations exhibit significant differences in metallicity below and above a critical redshift, ranging from approximately 1.5 to 2. The GRB production rate depends on the metallicity of the host galaxy [35]. To explore the potential differences between GRBs below and above the critical redshift, we aim to examine the variations in the Amati parameters with redshift. For this purpose, we divide the data sample (hereafter  $G$ ), containing 221 GRBs, into subgroups of low and high redshift. When the critical redshift is set at  $z = 1.5$ , the low- $z$  sample consists of 100 GRBs, with a median redshift of 0.90 and a redshift range of  $0.034 < z < 1.489$ . The high- $z$  sample comprises 121 GRBs, within a redshift range of  $1.517 < z < 8.2$  and a median redshift of 2.73. These subgroups are referred to as  $G_1$  and  $G_2$ , respectively. When the critical redshift is set at  $z = 2$ , the low- $z$  sample includes 132 GRBs, with a median redshift of 1.102 and a redshift range of  $0.034 < z < 1.98$ . The high- $z$  sample consists of 89 GRBs, within a redshift range of  $2.006 < z < 8.2$  and a median redshift of 3.09. These subgroups are referred to as  $G'_1$  and  $G'_2$ , respectively.

The observed values of the peak energy ( $E_{p,i}$ ) and isotropic-equivalent energy ( $E_{iso}$ ) along with their uncertainties, are available for all the GRBs in the data set. Since it is

advantageous to use the linear form of the Amati relation, i.e, Eq. 1.1 among the logarithm of the observational quantities, we define  $\chi^2$  as:

$$\chi^2 = \sum_{i=1}^N \left( \frac{g^i - f(E_{p,i}^i; a, b)}{\sigma^i} \right)^2, \quad (2.1)$$

where  $g^i = \log E_{\text{iso}}^i$ , is obtained from data, and  $f$  is the value of  $\log E_{\text{iso}}$  derived using Amati relation, i.e., corresponding to given  $E_{p,i}^i$  (see Eq. 1.1). The uncertainty  $\sigma^i$  in  $\log E_{\text{iso}}^i$  can be calculated as described in [22]:

$$\sigma_i^2 = (dE_{\text{iso}}/E_{\text{iso}})^2 + b^2(dE_{p,i}/E_{p,i})^2. \quad (2.2)$$

The likelihood,  $P(D|M)$ , which represents the probability of obtaining the data for the given model  $M$  can be expressed as:

$$P(D|M(a, b)) \propto e^{-\chi^2/2}, \quad (2.3)$$

where  $\chi^2$  is defined by Eq. 2.1. The best-fit values of the Amati parameters ( $a$  and  $b$ ) can be estimated by minimizing  $\chi^2$  in Eq. 2.1 or by maximizing likelihood in Eq. 2.3. However, this method does not provide direct probabilities of these parameters, thus we employ the Bayesian approach. The direct probability of the model  $M$ , also known as the posterior probability can be easily calculated using Bayes' theorem :

$$P(M(a, b)|D) \propto P(D|M(a, b))P(M(a, b)). \quad (2.4)$$

Here,  $P(M)$  represents the prior probability of the model. One should be cautious while selecting the prior probability as it can include personal biases and lead to an inappropriate posterior probability distribution. An advantage of the Bayesian approach is the ability to marginalize the undesired parameters. For example, marginalization on parameter  $b$  can be performed by integrating over it:

$$P(a|I) = \int P(I|a, b)P(a, b)db. \quad (2.5)$$

To determine whether the Amati parameters systematically increase or decrease with redshift, we fit the Amati relation in Eq. 1.1 for each subgroup of data using the aforementioned methods.

### 2.3 Distribution of Low and High- $z$ GRBs Across the Sky

GRB observations indicate a statistically isotropic distribution of their positions [36, 37]. A large number of GRBs is required to further investigate any potential deviations from isotropy [38]. To avoid any directional biases, we aim to ensure that our GRB sample and its subgroups adequately cover the sky. The positions of the 221 GRBs in our sample are plotted in Fig. 1, demonstrating fair sky coverage. Additionally, we plot the positions of low and high- $z$  GRBs separately in Fig. 2. Both subgroups exhibit fair sky coverage, indicating no clustering of GRBs in any particular region of the sky.

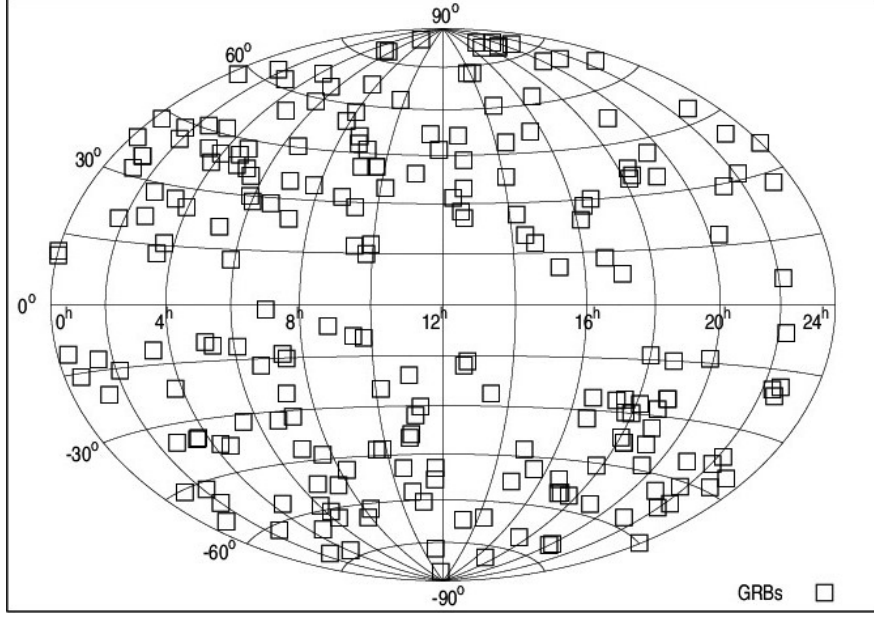


**Figure 1:** This celestial map shows the isotropic distribution of 221 gamma-ray bursts (GRBs) across the sky.

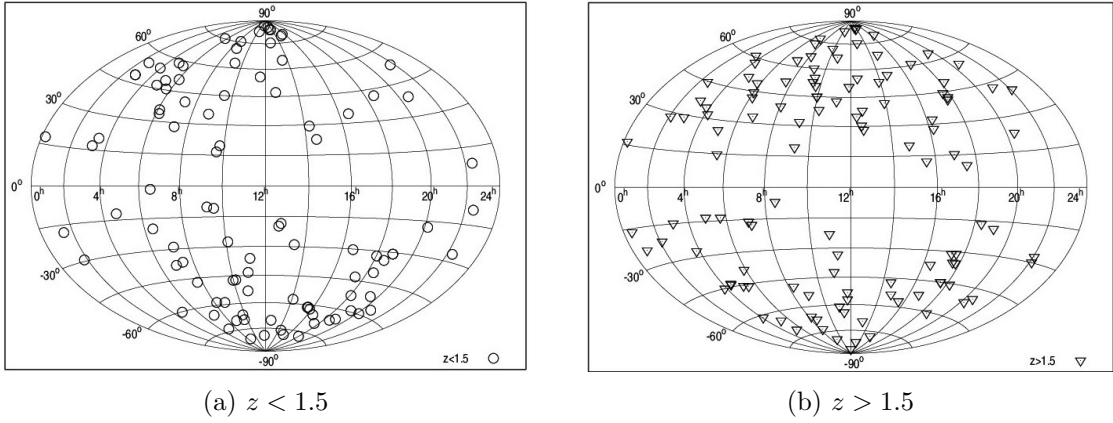


**Figure 2:** Distribution of the low and high- $z$  GRBs across the sky. Regardless of redshift, the distribution appears isotropic.

## 2.4 Intrinsic Scatter

The correlation between  $E_p$  and  $E_{iso}$  exhibits variability often attributed to inherent scatter [22, 39]. To mitigate this variability, we employ Reichart’s likelihood function, which incorporates the intrinsic scatter ( $\sigma_{int}$ ) along with the linear relation described by Eq. 1.1 and is given as

$$L_{Reichart}(a, b, \sigma_{int}) = \frac{1}{2} \frac{\sum \log(\sigma_{int}^2 + \sigma_{y_i}^2 + a^2 \sigma_{x_i}^2)}{\log(1 + a^2)} + \frac{1}{2} \sum \frac{(y_i - ax_i - b)^2}{\sigma_{int}^2 + \sigma_{x_i}^2 + a^2 \sigma_{x_i}^2}. \quad (2.6)$$

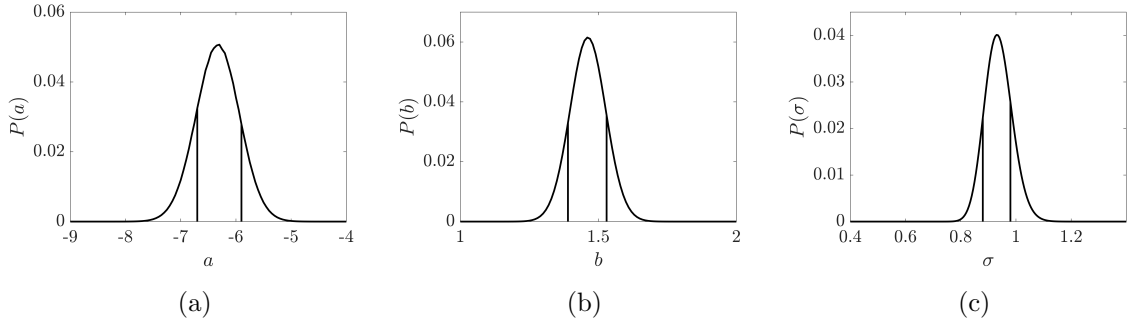


**Figure 3:** Distribution of posterior probability for Amati parameters  $a$ ,  $b$  and  $\sigma_{int}$  for data sample G (221 GRBs).

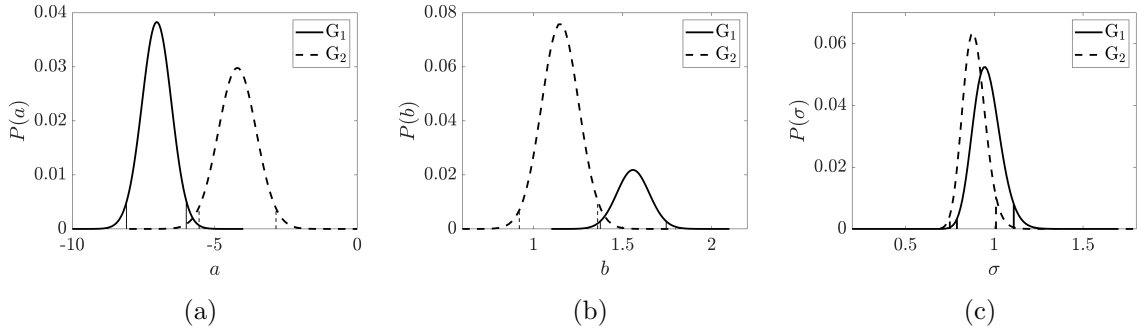


**Figure 4:** Posterior probability distributions of Amati parameters  $a$ ,  $b$  and  $\sigma_{int}$  for low- $z$  GRBs (group  $G_1$ ) and high- $z$  GRBs (group  $G_2$ ) with the threshold at  $z = 1.5$ . The low- $z$  and high- $z$  distributions are not in agreement and their difference is statistically significant at more than  $2\sigma$  confidence level for parameters  $a$  and  $b$ .

The correlation function,  $L_{Reichert}(a, b, \sigma_{int})$ , now involves three parameters. These parameters can be simultaneously fitted, or the parameter  $b$  can be analytically evaluated by setting  $\frac{\partial}{\partial b} L(a, b, \sigma_{int}) = 0$ . This yields:

$$b = \left[ \sum \frac{y_i - ax_i}{\sigma_{int}^2 + \sigma_{y_i}^2 + a^2 \sigma_{x_i}^2} \right] \left[ \sum \frac{1}{\sigma_{int}^2 + \sigma_{y_i}^2 + a^2 \sigma_{x_i}^2} \right]^{-1}. \quad (2.7)$$

To comprehend the impact of intrinsic scatter, we concurrently determine the optimal values for parameters  $a$ ,  $b$ , and  $\sigma_{int}$  using the aforementioned three-parameter likelihood function defined by Eq. 2.6. During the computation of the optimal value for one of the parameters, Bayesian marginalization is applied to the remaining two parameters. The same approach is applied to the different subgroups of the data as well.

### 3 Results and Discussion

In this section, we present our main results and highlight the possible instrumental biases that could be responsible for any differences between the low and high- $z$  GRB properties. Toward the end of the present section, we also discuss the main differences in the properties of host galaxies of low and high- $z$  long GRBs.

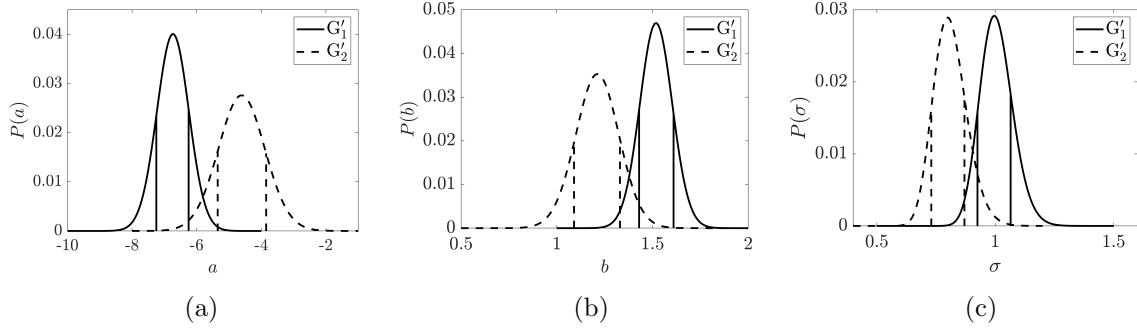


**Figure 5:** Posterior probability distributions of Amati parameters  $a$ ,  $b$  and  $\sigma_{int}$  for low- $z$  GRBs (group  $G'_1$ ) and high- $z$  GRBs (group  $G'_2$ ) with the threshold at  $z = 2$ . The low- $z$  and high- $z$  distributions are not in agreement and their difference is statistically significant at more than  $1\sigma$  confidence level for each parameter.

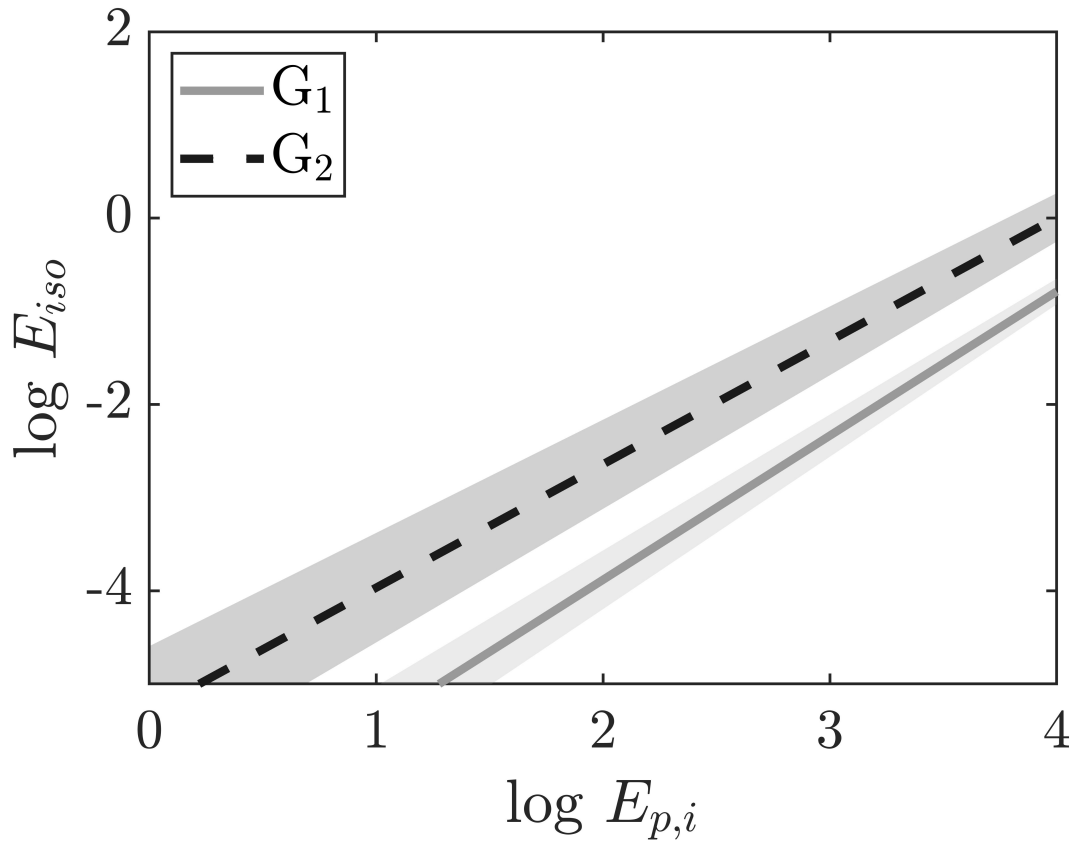


**Figure 6:** Straight line fit  $y = a + bx$  for the subgroups  $G_1$  and  $G_2$ , where  $a$  and  $b$  are the best-fit values of Amati parameters for 162 GRBs.



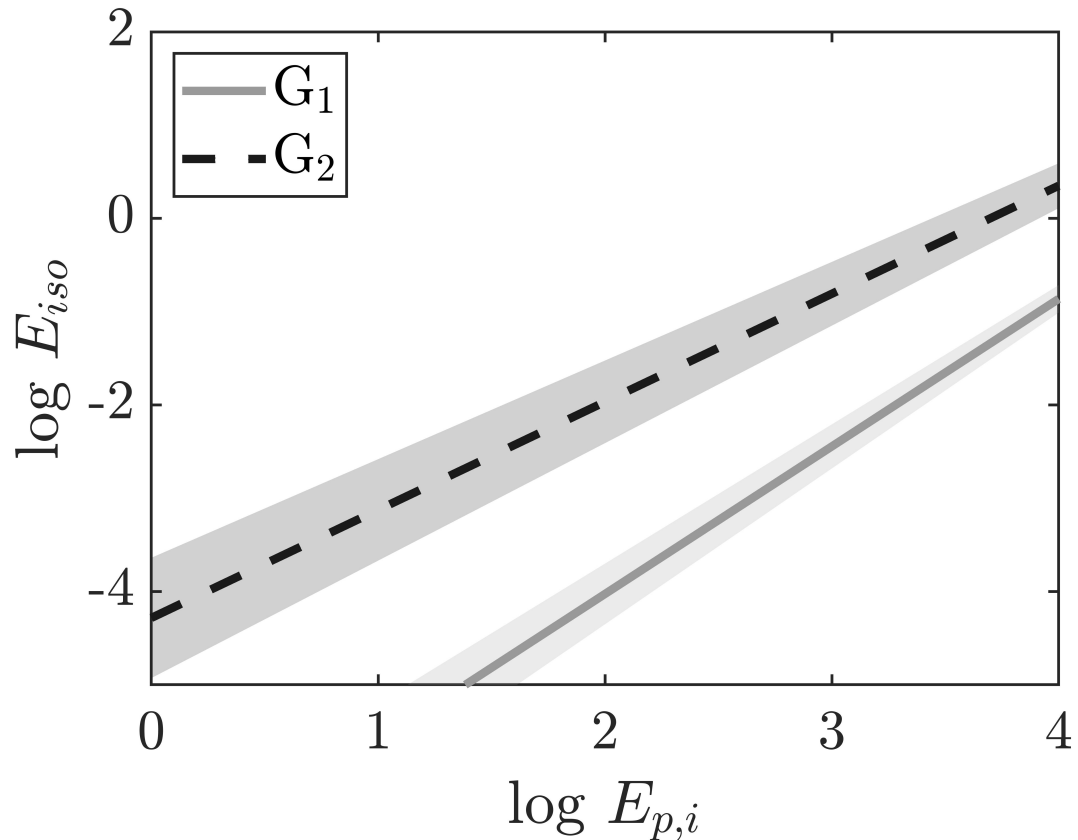


**Figure 7:** Straight line fit  $y = a + bx$  for the subgroups  $G_1$  and  $G_2$ , where  $a$  and  $b$  are the best-fit values of Amati parameters for 221GRB.

**Table 2:** Best-fit values of Amati parameters ( $a$ ,  $b$  and  $\sigma_{int}$ ) along with their  $1\sigma$  errors for data sample G (221 GRBs) and its subgroups  $G_1$  and  $G_2$ . The cut-off has been taken at  $z = 1.5$  to divide the data into subgroups. The Bayesian marginalization has been employed to determine the best-fit value of each parameter.

Data Set	$a$	$b$	$\sigma_{int}$
G	$-6.30 \pm 0.40$	$1.46 \pm 0.07$	$0.93 \pm 0.05$
$G_1(100)$	$-7.05 \pm 0.55$	$1.56 \pm 0.09$	$0.95 \pm 0.08$
$G_2(121)$	$-4.20 \pm 0.70$	$1.14 \pm 0.12$	$0.88 \pm 0.07$

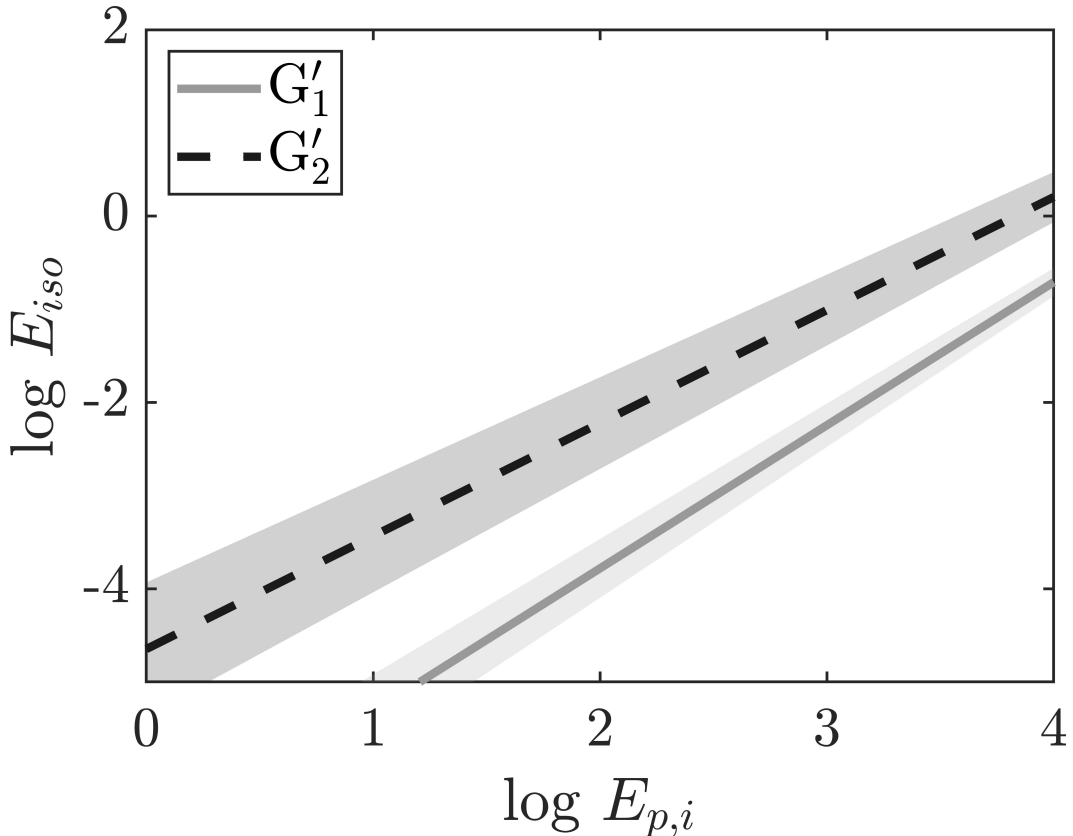


**Figure 8:** Straight line fit  $y = a + bx$  for the subgroups  $G'_1$  and  $G'_2$ , where  $a$  and  $b$  are the best-fit values of Amati parameters for 221GRB.

**Table 3:** Best-fit values of  $a$ ,  $b$  and  $\sigma_{int}$  along with their  $1\sigma$  errors for the subgroups  $G'_1$  and  $G'_2$ . The cut-off has been taken at  $z = 2$  to divide the data into subgroups. The Bayesian marginalization has been employed to determine the best-fit value of each parameter.

Data Set	$a$	$b$	$\sigma_{int}$
$G'_1$	$-6.75 \pm 0.50$	$1.52 \pm 0.09$	$0.99 \pm 0.07$
$G'_2$	$-4.60 \pm 0.75$	$1.21 \pm 0.12$	$0.80 \pm 0.07$

### 3.1 Main Results

The optimal parameters of the Amati relation are derived through a Bayesian approach, yielding the best-fit values and their associated  $1\sigma$  uncertainties for the comprehensive dataset  $G$ , as summarized in Table 2. Notably, the intercept ( $a$ ) of the linear Amati relation exhibits a negative value, while its slope demonstrates a positive trend. The intrinsic scatter remains consistently below unity across all instances. Figure 3 visually represents the probability distribution of the three parameters, with vertical lines denoting the  $1\sigma$  confidence level.

Table 2 also presents the optimal parameters, namely  $a$  and  $b$ , for the distinct subgroups

$G_1$  and  $G_2$  (with the threshold at  $z = 1.5$ ). The intercept is still negative and the slope is positive in both subgroups. Figure 4 illustrates the probability distributions associated with these subgroups, delineating the distinctive nature of  $G_1$  and  $G_2$ . Vertical lines are employed to mark the  $2\sigma$  confidence level. Notably, the values of  $a$  and  $b$  exhibit a discrepancy exceeding the  $2\sigma$  threshold, indicating a discernible distinction in the GRB populations at low and high redshifts. Despite a smaller intrinsic scatter observed at high redshifts, the disparity is not statistically significant.

Table 3 presents the optimal values of  $a$  and  $b$ , for the subgroups  $G'_1$  and  $G'_2$  (with the threshold at  $z = 2$ ). Their  $1\sigma$  errors have also been shown in the respective columns. The continuously negative intercept and positive slope observed in both subgroups underscore a consistent trend. The corresponding posterior probability distributions for these parameters have been shown in Figure 5. The vertical lines have been drawn at  $1\sigma$  level. The significance is comparatively smaller in this case however, it is still at more than  $1\sigma$  for both  $a$  and  $b$ . In this case, the intrinsic scatter is also significantly different for the two subgroups.

### 3.2 Probable Instrumental Biases and Selection Effects

Possible biases in each instrument could arise due to their design, calibration, and operational characteristics which may be partly responsible for the observed differences in GRB populations. BAT [40] may exhibit biases related to its coded aperture imaging technique, potentially leading to systematic errors in position determination. It can affect the identification of the host galaxy and hence the redshift measurement. Another issue with the BAT instrument is its capability to detect energies up to 150 keV only [33], which is less than the average peak energy of GRBs [41]. Thus, for several Swift observed GRBs, it is not possible to directly determine the fluence and  $E_{p,obs}$ . FGST's LAT may face biases due to background noise, energy calibration uncertainties, and instrument response variations across its wide energy range. GBM's biases could include sensitivity variations across its energy range and potential systematic errors in event classification. While these instruments provide invaluable data, understanding and mitigating biases are crucial for accurate gamma-ray observations.

### 3.3 Low- $z$ vs High- $z$ GRB Hosts

As mentioned in 3.1, we observe significant differences in best-fit values of Amati parameters for low and high- $z$  GRB subgroups. Below we analyse our results in the context of differences in the low- $z$  and high- $z$  GRB host galaxies.

In a detailed study [32] and [42] claim that at high  $z$ , long GRBs host galaxies include all morphological types including early-type galaxies. This could be because at high  $z$  the early-type galaxies can be observed during their active star formation period. In contrast, star formation in the early-type galaxies at low  $z$  is often quenched.

High- $z$  GRB hosts are younger and thus have low metallicities. On the other hand, low- $z$  hosts, especially the early-type ones, are older and have higher metallicities [32]. These differences underscore significant evolutionary changes in galaxy properties and environments from high to low redshifts, affecting the nature and identification of long GRB host galaxies. At a given redshift, dust-obscured GRB hosts are more massive than optically bright galaxies, with massive GRB hosts becoming fairly common at  $z > 1.5$  [43]. The authors also link the smaller GRB production at low redshift to metallicity. Using the optically unbiased GRB host (TOUGH) Survey [44] claims that GRB hosts at high  $z$  are faint and low in metallicity [45] The studies based on Damped Lyman  $\alpha$  systems at high  $z$  support the existence of two GRB progenitor channels, with one being mildly influenced by metallicity [45].

## 4 Conclusions

In our study, we analyzed 221 long GRBs across a broad redshift range, dividing the sample into two groups based on a critical redshift,  $z_{crit}$ , set at 1.5 and 2.0. By fitting the Amati relation to each subgroup, we observed variations in the fitting parameters “ $a$ ” and “ $b$ ” relative to redshift. With  $z_{crit} = 1.5$ , the parameters for the low and high- $z$  subgroups show a difference of approximately  $2\sigma$ , while the intrinsic scatter remains within  $1\sigma$ . Increasing  $z_{crit}$  to 2.0, the differences in all parameters exceed  $1\sigma$ , suggesting a statistically significant difference between the low and high- $z$  GRBs. The difference may be inherent to the properties of hosts such as metallicity. Alternatively, the differences may arise due to selection effects or instrumental biases. These findings align with [22], who reported similar discrepancies using a different dataset at  $z_{crit} = 1.5$ . To date, several researchers have explored various aspects of GRB energy and luminosity correlations including the redshift evolution of these relationships. One of the first to do so, [23], used 48 GRBs to suggest that the Amati relation steepens with redshift. This conclusion was initially questioned by a later study by [46], which expanded the dataset to 76 bursts and suggested that the earlier findings might be an artefact of the small sample size. More recent investigations, including that of [47] and [14], have corroborated the evolving nature of the Amati relation across different energy scales and redshifts, highlighting significant shifts in GRB luminosity correlations over time. These results underscore the non-universality of the Amati relation and challenge its use in standard GRB calibration methods. Looking forward, missions like the Transient High-Energy Sky and Early Universe Surveyor (THESEUS), scheduled for launch in 2032 [48], and the enhanced X-ray Timing and Polarimetry mission, eXTP, [49], promise to enhance our understanding greatly. With their unprecedented sensitivity and observational capabilities, these missions are expected to observe high- $z$  GRBs up to  $z = 12$  and detect about 100 GRBs per year, respectively. The increased accuracy and expanded dataset from these missions will provide more robust statistical validation of our findings and further elucidate the differences between low and high- $z$  GRB populations. This evidence supports the hypothesis that the Amati relation is dynamic, reflecting more profound cosmological phenomena than previously understood. As such, our study contributes to the ongoing discourse on the complex behaviour of cosmic events, paving the way for future explorations that might redefine our understanding of the universe’s most energetic phenomena.

## References

- [1] D. Band, J. Matteson, L. Ford, B. Schaefer and et al., *Batse observations of gamma-ray burst spectra. i. spectral diversity*, *The Astrophysical Journal* **413** (1993) 281.
- [2] P. Kumar and B. Zhang, *The physics of gamma-ray bursts and relativistic jets*, *Physics Reports* **561** (2014) 1.
- [3] C. Kouveliotou, C.A. Meegan, G.J. Fishman, N.P. Bhat and et al., *Identification of two classes of gamma-ray bursts*, *Astrophysical Journal Letters* **413** (1993) L101.
- [4] L. Amati, *To be short or long is not the question*, *Nature Astronomy* **5** (2021) 877.
- [5] L. Amati, F. Frontera, M. Tavani, J.J.M. in ’t Zand and et al., *Intrinsic spectra and energetics of bepposax gamma-ray bursts with known redshifts*, *Monthly Notices of the Royal Astronomical Society* **390** (2002) 81.

- [6] L. Amati, *The  $E_{p,i} - E_{iso}$  correlation in gamma-ray bursts: updated observational status, re-analysis and main implications*, *Monthly Notices of the Royal Astronomical Society* **372** (2006) 233.
- [7] L. Amati, C. Guidorzi, F. Frontera, M.D. Valle and et al., *Measuring the cosmological parameters with the  $E_{p,i} - E_{iso}$  correlation of gamma-ray bursts*, *Monthly Notices of the Royal Astronomical Society* **391** (2008) 577.
- [8] L. Amati, F. Frontera and C. Guidorzi, *Extremely energetic fermi gamma-ray bursts obey spectral energy correlations*, *Astronomy & Astrophysics* **508** (2009) 173.
- [9] D. Yonetoku, T. Murakami, T. Nakamura, R. Yamazaki and et al., *Gamma-ray burst formation rate inferred from the spectral peak energy–peak luminosity relation*, *The Astrophysical Journal* **609** (2009) 635.
- [10] G. Ghirlanda, G. Ghisellini, D. Lazzati and C. Firmani, *Gamma ray bursts: New rulers to measure the universe*, *The Astrophysical Journal* **613** (2004) L13.
- [11] G. Ghirlanda, L. Nava and G. Ghisellini, *Spectral-luminosity relation within individual fermi gamma rays bursts*, *Astronomy & Astrophysics* **511** (2010) A43.
- [12] M.G. Dainotti, V. Nielson, G. Sarracino, E. Rinaldi and et al., *Optical and x-ray grb fundamental planes as cosmological distance indicators*, *Monthly Notices of the Royal Astronomical Society* **514** (2022) 1828.
- [13] Y. Dai, X.-G. Zheng, Z.-X. Li and H.G. et al., *Redshift evolution of the amati relation: Calibrated results from the hubble diagram of quasars at high redshifts*, *Astronomy & Astrophysics* **651** (2021) L8.
- [14] L. Huang, Z. Huang, X. Luo, X. He and et al., *Reconciling low and high redshift grb luminosity correlations*, *Physical Review D* **103** (2021) 123521.
- [15] R. Basak and A.R. Rao, *Pulse-wise amati correlation in fermi gamma-ray bursts*, *Monthly Notices of the Royal Astronomical Society: Letters* **436** (2013) 3082.
- [16] F. Daigne, E.M. Rossi and R. Mochkovitch, *The redshift distribution of swift gamma-ray bursts: evidence for evolution*, *Monthly Notices of the Royal Astronomical Society* **372** (2006) 1034.
- [17] X.D. Jia, J.P. Hu, J. Yang, B.B. Zhang and et al., *The  $E_{p,i} - E_{iso}$  correlation of gamma-ray bursts: calibration and cosmological applications*, *Monthly Notices of the Royal Astronomical Society* **516** (2022) 2575.
- [18] N. Khadka, O. Luongo, M. Muccino and B. Ratra, *Do gamma-ray burst measurements provide a useful test of cosmological models*, *Journal of Cosmology and Astroparticle Physics* (2021) 42.
- [19] M. Demianski, E. Piedipalumbo, D. Sawant and L. Amati, *Cosmology with gamma-ray bursts: I. the hubble diagram through the calibrated  $e_{p,i} - e_{iso}$  correlation*, *Astronomy & Astrophysics* **598** (2017) A112.
- [20] S. Cao, N. Khadka and B. Ratra, *Standardizing dainotti-correlated gamma-ray bursts, and using them with standardized amati-correlated gamma-ray bursts to constrain cosmological model parameters*, *Monthly Notices of the Royal Astronomical Society* **510** (2021) 2928.
- [21] M.G. Dainotti, V.F. Cardone, E. Piedipalumbo and S. Capozziello, *Slope evolution of grb correlations and cosmology*, *Monthly Notices of the Royal Astronomical Society* **436** (2013) 82.
- [22] M. Singh, D. Singh, D. Verma and et al., *Investigating the evolution of amati parameters with redshift*, *Research in Astronomy and Astrophysics* **24** (2024) 015015.
- [23] Li-Xin Li, *Variation of the amati relation with cosmological redshift: a selection effect or an evolution effect?*, *Monthly Notices of the Royal Astronomical Society: Letters* **379** (2007) L55.
- [24] J.J. Geng and Y.F. Huang, *On the correlation of low-energy spectral indices and redshifts of gamma-ray bursts*, *The Astrophysical Journal* **764** (2013) 75.

- [25] R. Tsutsui, D. Yonetoku, T. Nakamura, K. Takahashi and et al., *Possible existence of the  $E_p - L_p$  and  $E_p, i - E_{iso}$  correlations for short gamma-ray bursts with a factor 5–100 dimmer than those for long gamma-ray bursts*, *Monthly Notices of the Royal Astronomical Society* **431** (2013) 1398.
- [26] N.R. Butler, D. Kocevski and J.S. Bloom, *Generalized tests for selection effects in gamma-ray burst high-energy correlations*, *The Astrophysical Journal* **694** (2009) 76.
- [27] H. Zitouni, N. Guessoum and W.J. Azzam, *Revisiting the amati and yonetoku correlations with swift grbs*, *Astrophysics and Space Science* **351** (2014) 267.
- [28] A. Mortlock, C.J. Conselice, W.G. Hartley, J.R. Owersworth and et al., *The redshift and mass dependence on the formation of the hubble sequence at  $z > 1$  from candles/uds*, *Monthly Notices of the Royal Astronomical Society* **434** (2013) 1185.
- [29] C.J. Conselice, *The evolution of galaxy structure over cosmic time*, *Astronomy and Astrophysics* **52** (2014) 291.
- [30] L. Ferreira, C.J. Conselice, E. Sazonova, F. Ferrari and et al., *The just hubble sequence: The rest-frame optical evolution of galaxy structure at  $1.5 < z < 8$* , *The Astrophysical Journal* **938** (2022) L2.
- [31] F.Y. Wang and Z.G. Dai, *Long grbs are metallicity-biased tracers of star formation: evidence from host galaxies and redshift distribution*, *The American Astronomical Society* **213** (2014) 15.
- [32] M. Palla, F. Matteucci, F. Calura and F. Longo, *Galactic archaeology at high redshift: Inferring the nature of grb host galaxies from abundances*, *The Astrophysical Journal* **889** (2020) 4.
- [33] N. Gehrels, G. Chincarini, P. Giommi, K.O. Mason and et al., *The swift gamma-ray burst mission*, *The Astrophysical Journal* **611** (2011) 1005.
- [34] W.B. Atwood, A.A. Abdo, M. Ackermann and W.A. et al., *The large area telescope on the fermi gamma-ray space telescope mission*, *The Astrophysical Journal* **697** (2009) 1071.
- [35] D.A. Perley, T. Krühler, S. Schulze and A. de Ugarte Postigo et al., *The swift gamma-ray burst host galaxy legacy survey - i. sample selection and redshift distribution*, *The Astrophysical Journal* **817** (2016) 7.
- [36] U. Andrade, C.A.P. Bengaly, J.S. Alcaniz and S. Capozziello, *Revisiting the statistical isotropy of grb sky distribution*, *Monthly Notices of the Royal Astronomical Society* **490** (2019) 4481.
- [37] L.G. Balazs, A. Meszaros and I. Horvath, *Anisotropy of the sky distribution of gamma-ray bursts*, *Astronomy & Astrophysics* **339** (1998) 1.
- [38] S.K. Sethi, S.G. Bhargavi and J. Greiner, *On the clustering of grbs on the sky*, *AIP Conference Proceedings* **526** (2000) 107.
- [39] D.E. Reichart, D.Q. Lamb, E.E. Fenimore, E. Ramirez-Ruiz and et al., *A possible cepheid-like luminosity estimator for the long gamma-ray bursts*, *The Astrophysical Journal* **552** (2001) 57.
- [40] S.D. Barthelmy, L.M. Barbier, J.R. Cummings, E.E. Fenimore and et al., *The burst alert telescope (bat) on the swift midex mission*, *Space Science Reviews* **120** (2005) 143.
- [41] Y. Kaneko, R.D. Preece, M.S. Briggs, W.S. Paciesas and et al., *The complete spectral catalog of bright batse gamma-ray bursts*, *Astrophysical Journal Supplement Series* **166** (2006) 298.
- [42] V. Grieco, F. Matteucci, F. Calura, S. Boissier and et al., *Chemical evolution models: Grb host identification and cosmic dust predictions*, *Monthly Notices of the Royal Astronomical Society* **444** (2014) 1054.
- [43] D.A. Perley, A.J. Levan, N.R. Tanvir and S.B.C. et al., *A population of massive, luminous galaxies hosting heavily dust-obscured gamma-ray bursts: implications for the use of grbs as tracers of cosmic star formation*, *The Astrophysical Journal* **778** (2013) 128.

- [44] S. Schulze, R. Chapman, J. Hjorth, A.J. Levan and et al., *The optically unbiased grb host (tough) survey. vii. the host galaxy luminosity function: probing the relationship between grbs and star formation to redshift 6*, *The Astrophysical Journal* **808** (2015) 73.
- [45] A. Cucchiara, M. Fumagalli, M. Rafelski, D. Kocevski and et al., *Unveiling the secrets of metallicity and massive star formation using dlas along gamma-ray bursts*, *Astrophysical Journal* **804** (2015) 16.
- [46] G. Ghirlanda, L. Nava, G. Ghisellini, C. Firmani and et al., *The epeak–eiso plane of long gamma-ray bursts and selection effects*, *Monthly Notices of the Royal Astronomical Society* **387** (2008) 319.
- [47] G.J. Wang, H. Yu, Zheng-Xiang and J.-Q.X. et al., *Evolutions and calibrations of long gamma-ray-burst luminosity correlations revisited*, *The Astrophysical Journal* **836** (2017) 103.
- [48] G. Ghirlanda, R. Salvaterra, M. Toffano, S. Ronchini and et al., *Gamma ray burst studies with theseus*, *Experimental Astronomy* **52** (2021) 277.
- [49] S.N. Zhang and A.S.M.F.Y.X. et al., *The enhanced x-ray timing and polarimetry mission—extp*, *Science China Physics, Mechanics, and Astronomy* **62** (2019) 29502.